Electronic Supplementary Material (ESI) for Physical Chemistry Chemical Physics.

Supporting Information: Nano-protrusions in intercalated graphite: understanding the structural and electronic effects through DFT

Hussam Bouaamlat[a*], Ari Paavo Seitsonen[b], Gianlorenzo Bussetti[c]
Rossella Yivlialin[c], Stefania De Rosa[e], Paolo Branchini[a]
and Luca Tortora[a,d*]
[a]LASR3 Surface Analysis Laboratory-National Institute for Nuclear Physics
RomaTre, via della Vasca Navale 84, Rome I-00146, Italy
[b]Département de Chimie, École Normale Supérieure, 24 rue Lhomond,
F-75005 Paris, France
[c]Department of Physics, Politecnico di Milano, p.za Leonardo da Vinci 32,
Milano I-20133, Italy
[d]Department of Science, Roma Tre University, via della Vasca Navale 84,
Rome I-00146, Italy
[e]Université Grenoble Alpes, CNRS, Grenoble INP, LGP2, 38000 Grenoble, France

*Corresponding Authors:
Email: luca.tortora@uniroma3.it
hussam.bouaamlat@infn.it

In the accompanying supporting material file, we have included additional figures for the main text and supplementary notes that provide further depth to our research:

- Section I, Supplementary Figures: These are the essential figures that supplement and provide a visual complement to the main text.
- Section II, Supplementary Note 1: This section delves into a comprehensive breakdown of the energy components of the intercalation and adhesion energies used in the main text.
- Section III, Supplementary Note 2: Here, we discuss the implications of utilizing different coverage areas, such as 6×6 and 10×10, in comparison to the 12×12 system examined in the main text.
- Section IV, Supplementary Note 3: In this section, we present a hypothetical qualitative discussion on the implementation of microsolvation, examining the influence of incorporating explicit solvation molecules on the properties of the bilayer graphene system.

We have included the last part separately from the main text as we believe it better fits within the supporting material file.

I Supplementary Figures

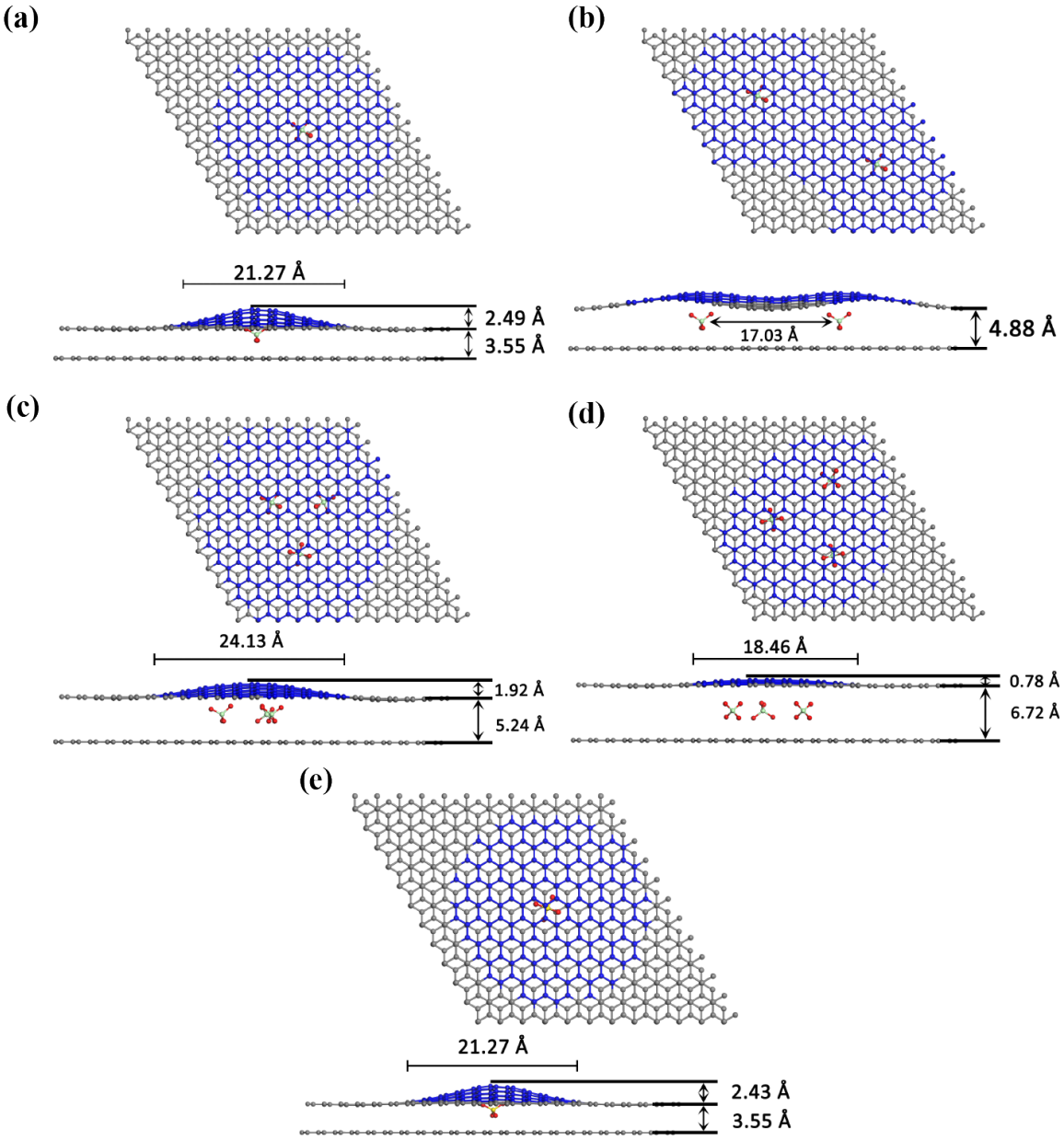

Figure S1: DFT models of single SO_4^{2-} and single and multiple ClO_4^- anions intercalated between two graphene layers; side and top view with the blue atoms indicate the deformed graphene regions. We defined the deformed region highlighted in blue by selecting the C atoms whose z coordinates fulfill the condition $z > h_{\min} + 0.4$ Å. (a) 1-ClO_4^-, (b) 2-ClO_4^--L, (c) 3-ClO_4^--S, (d) 3-ClO_4^--L, and (e) 1-SO_4^{2-}.

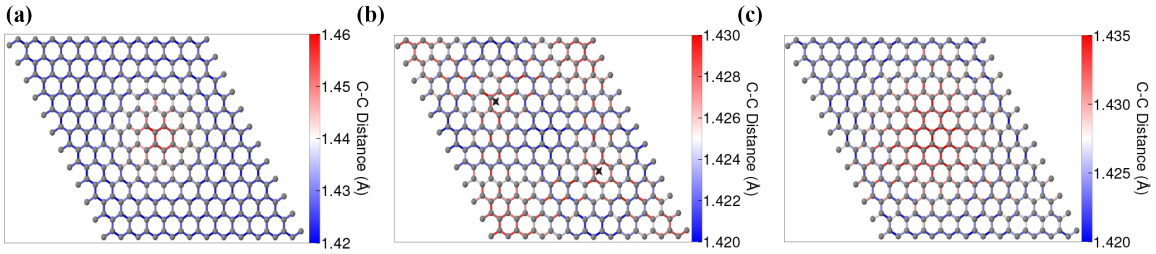

Figure S2: The C-C bonds of the upper layer are colored according to the bond length from blue to red in (a) 1-ClO_4^-, (b) 2-ClO_4^--L, and (c) 3-ClO_4^--S. The two black stars in (b) indicates the position of the anion below the layer. 3-ClO_4^--L structure is not shown because the changes in the bonds are negligible. The length scales are different.

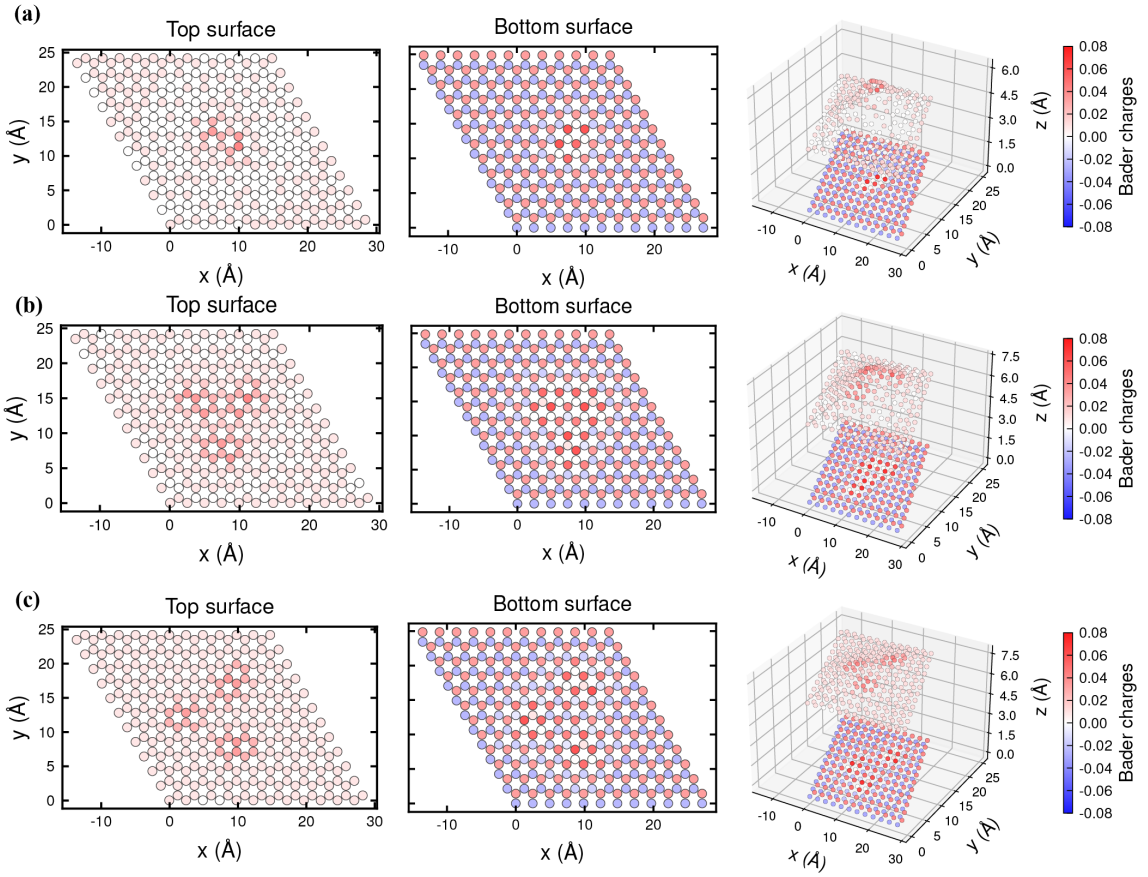

Figure S3: The distribution of Bader charges in (a) 1-ClO_4^-, (b) 3-ClO_4^--S, and (c) 3-ClO_4^--L in color code as evaluated using the Critic2 code.

Table S1: The Values of Bader Charges Before and After Intercalation in All Structures

Structures	Sum over C atoms	Top layer	Bottom layer	Sum over ClO_4^-	Avg. over O atoms	Cl atoms
Pristine bilayer	-0.003	-0.002	-0.001	-	-	-
ClO_4 neutral	-	-	-	0	-0.602	2.410
1-ClO_4^-	0.864	0.370	0.494	-0.867	-0.842	2.502
2-ClO_4^--S	1.762	0.842	0.920	-0.883	-0.827	2.426
2-ClO_4^--L	1.803	0.885	0.919	-0.903	-0.826	2.401
3-ClO_4^--S	2.685	1.338	1.347	-0.899	-0.822	2.391
3-ClO_4^--L	2.792	1.416	1.376	-0.933	-0.821	2.346

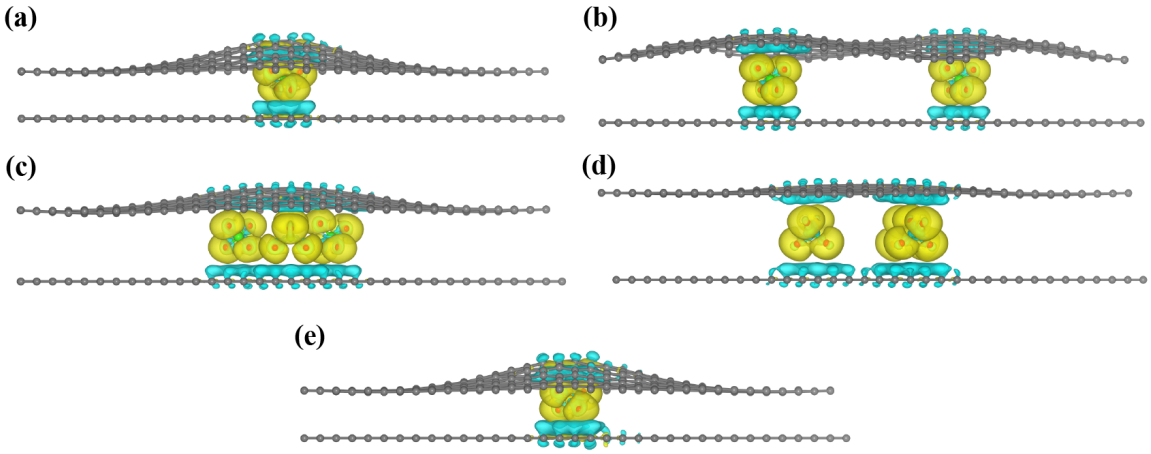

Figure S4: Charge density difference of (a) 1-ClO_4^-, (b) 2-ClO_4^--L, (c) 3-ClO_4^--S, (d) 3-ClO_4^--L, and (e) 1-SO_4^{2-}. The yellow and cyan areas indicate electron accumulation and depletion, respectively. Isosurface level is set to $\pm 6 \times 10^{-3}$ e/Å^3.

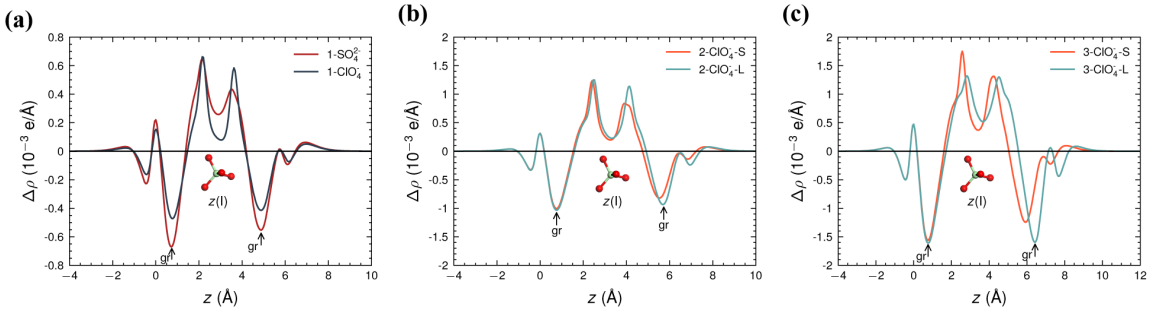

Figure S5: Planar-averaged charge density difference in the planes parallel to the graphene surface as a function of the z-coordinate in (a) 1-ClO_4^- and 1-SO_4^{2-}, (b) 2-ClO_4^--S and 2-ClO_4^--L, (c) 3-ClO_4^--S and 3-ClO_4^--L, with z(I) as the position of ions.

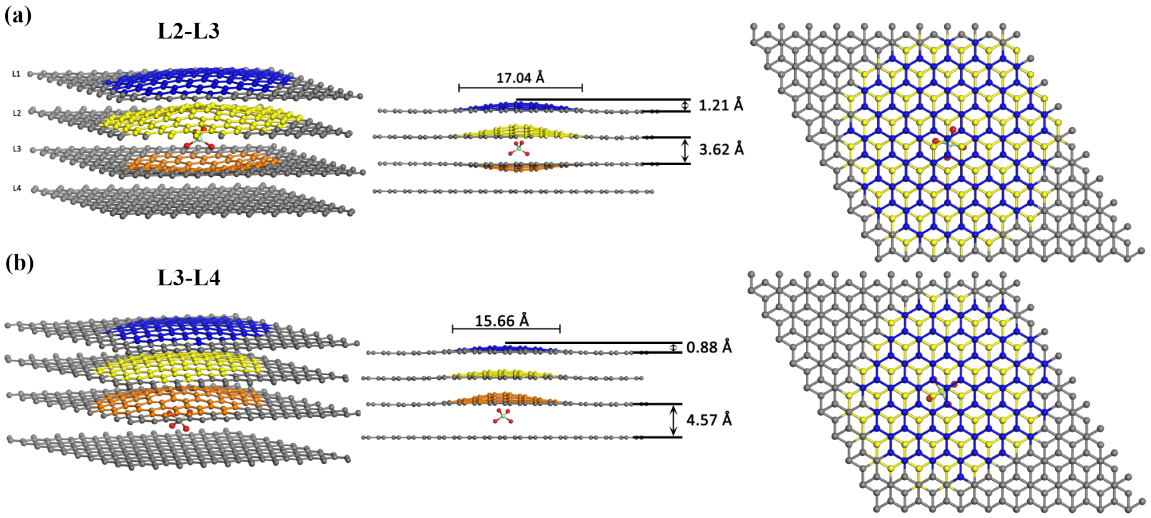

Figure S6: The side and top view of ClO_4^- intercalated in a 10×10 4-layer graphite slab. The ClO_4^- is intercalated between (a) the second and the third and (b) the third and the fourth layers. The colored carbon atoms in different layers correspond to the vertical deformations caused by the anion.

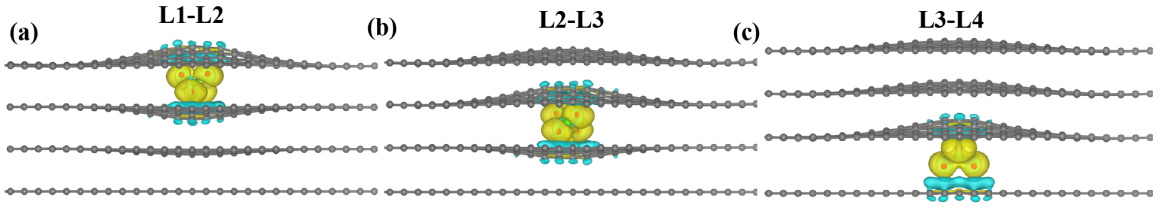

Figure S7: Charge density difference of ClO_4^- intercalated between (a) the first and the second, (b) the second and third, and (c) the third and the fourth layers. The yellow and cyan areas indicate electron accumulation and depletion, respectively. Isosurface level is set to $\pm 6 \times 10^{-3}$ e/Å^3.

Table S2: Structural and Energetic Characteristics of the Multilayer Systems. Nanoprotrusion Height (h_{nano}), Minimum Interlayer Distance (h_{min}), Adhesion Energy (E_{adh}), Intercalation Energy per Anion $\left(\bar{E}_{\mathrm{ic}}\right)$, Total Intercalation Energy (E_{ic}). All Energies are Expressed in eV and Heights in Å.

Structures	h_{nano}	h_{min}	D	E_{adh}	$\bar{E}_{\mathrm{ic}}$	E_{ic}
L1-L2	1.78	3.51	11.02	5.74	3.16	3.16
L2-L3	1.21	3.62	11.28	5.62	4.26	4.26
L3-L4	0.88	4.57	11.91	2.66	6.09	6.09
L1-L2-S	1.97	3.65	11.38	5.09	1.62	3.24
L1-L2-L	1.60	3.95	11.85	2.83	2.13	4.27
L2-L3-S	1.22	4.17	11.95	3.67	2.35	4.70
L2-L3-L	0	6.80	14.06	1.42	2.05	4.11
L3-L4-S	0	7.45	14.60	1.46	1.95	3.91
L3-L4-L	0	7.34	14.42	1.49	1.93	3.87

II Supplementary Note 1: Decomposition of the Energies

In order to deepen our understanding of the different physical quantities that underpin the intercalation process, we derived decompositions of the two main energy quantities, the intercalation and adhesion energies. Here we give the derivations and some further comments. We use the notation where $E(S)$ is the total energy of the system, $S[\mathrm{I}]_x$ is the collection of the x (an)ions, where x is the count of anions, a superscript asterisk $*$ denotes that the coordinates of the subsystem have been extracted from the geometry of the full intercalated system – otherwise the geometry is optimized to yield the lowest total energy –, underlined terms in equations are combined in the subsequent expressions.

II.I Intercalation

We start by defining the intercalation energy as

$$E_{\mathrm{ic}} = E\left(\mathrm{gr}[\mathrm{I}]_x\right) - \left[E(\mathrm{gr}) + E\left(x[\mathrm{I}]_1\right)\right],$$

where $E\left(\mathrm{gr}[\mathrm{I}]_x\right), E(\mathrm{gr})$ and $E(x[\mathrm{I}]_1)$ are the total energies of the intercalated system, the bilayer graphene, and the x ions, respectively. We define the energy of the ionic system as the sum of the total energies of each of the optimised ions, or,

$$E\left(x[\mathrm{I}]_1\right) = x \times E\left([\mathrm{I}]_1\right)$$

Further we define an energy of the ionic arrangement in the intercalated system as the sum over the total energy of each isolated ion in the system in the geometry extracted from the intercalated system, $E\left(x[\mathrm{I}]_1^*\right) = \Sigma E\left([\mathrm{I}]_1^*\right)$.

By adding and subtracting the same terms one can split the E_{ic} as

$$E_{\mathrm{ic}} = E\left(\mathrm{gr}[\mathrm{I}]_x\right) \underline{-E(\mathrm{gr}) + E\left(\mathrm{gr}^*\right)} - E\left(\mathrm{gr}^*\right) \underline{-E\left(x[\mathrm{I}]_1\right) + E\left(x[\mathrm{I}]_1^*\right)} - E\left(x[\mathrm{I}]_1^*\right)$$

where the last two terms are the energies of the rigid isolated systems in the geometry of the intercalated ion; then one defines

$$E_{\mathrm{int}} = E\left(\mathrm{gr}[\mathrm{I}]_x\right) - E\left(\mathrm{gr}^*\right) - E\left(x[\mathrm{I}]_1^*\right)$$

as the interaction between the ions and the graphite substrate, in the geometry of the

intercalated system, and

$$E_{\mathrm{elas}}(\mathrm{I}) = -E\left(x[\mathrm{I}]_1\right) + E\left(x[\mathrm{I}]_1^*\right)$$
$$E_{\mathrm{elas}}(\mathrm{gr}) = -E(\mathrm{gr}) + E\left(\mathrm{gr}^*\right),$$

which characterise the elastic energy that one has to insert into the system to attain the adsorption geometry. Thus after reordering and combining the terms we eventually arrive at the decomposition of the intercalation energy as

$$E_{\mathrm{ic}} = E_{\mathrm{int}} + \left[E_{\mathrm{elas}}(\mathrm{gr}) + E_{\mathrm{elas}}(\mathrm{I})\right].$$

The first term, E_{int}, is usually negative and describes the attraction between the ions and the substrate. The two other terms are always positive and account for the energy penalty to deform the subsystems from the optimal geometry into the corresponding geometries in the intercalated system. Empirically we notice that the term $E_{\mathrm{elas}}(\mathrm{I})$ is much smaller and varies less than the other terms, and thus $E_{\mathrm{ic}} \cong E_{\mathrm{int}} + E_{\mathrm{elas}}(\mathrm{gr})$, a sum of two terms with opposite signs.

We note that we can study further the role of the different energy contributions in the ions without the substrate of the bilayer graphene in detail. In addition to the total energy of the independent, optimised ions from above, $E\left(x[\mathrm{I}]_1\right) = x \times E\left([\mathrm{I}]_1\right)$, and the sum over the rigid ions in the total system, $E\left(x[\mathrm{I}]_1^*\right) = \Sigma E\left([\mathrm{I}]_1^*\right)$, we use the energy of the ions all in the same calculation, $E\left([\mathrm{I}]_x^*\right)$. We further comment that in the case of three ions one could further inspect the role of super-molecular interactions by dividing the energy to one-, two- and three-body interactions, but we do not delve into this here, as the other results already indicate a weak ion-ion interactions in the systems under investigation here.

Adding and subtracting the energy of the ionic system interacting in the geometry of the full system, $E\left([\mathrm{I}]_x^*\right)$, from the elastic energy of the ions we obtain

$$\begin{aligned} E_{\mathrm{elas}}(\mathrm{I}) &= -E\left(x[\mathrm{I}]_1\right) + E\left(x[\mathrm{I}]_1^*\right) \\ &= \underline{-E\left(x[\mathrm{I}]_1\right) + E\left([\mathrm{I}]_{\mathrm{x}}^*\right)}\ \underline{-E\left([\mathrm{I}]_{\mathrm{x}}^*\right) + \mathrm{E}\left(x[\mathrm{I}]_1^*\right)} \\ &= E_{\mathrm{bind}}(\mathrm{I}) - E_{\mathrm{int}}(\mathrm{I}) \end{aligned}$$

where we have defined the two new terms

$$E_{\mathrm{bind}}(\mathrm{I}) = E\left([\mathrm{I}]_x^*\right) - E\left(x[\mathrm{I}]_1\right)$$

and

$$E_{\text{int}}(\text{I}) = E\left([\text{I}]_x^*\right) - E\left(x[\text{I}]_1^*\right).$$

The first quantity, $E_{\text{bind}}(\text{I})$, quantifies the interaction energy between the ions at the same geometries but once interacting and once without the inter-molecular interaction excluded. The second quantity, $E_{\text{int}}(\text{I})$, characterises the full interaction among the ions, bringing them from the gas phase to the intercalated system (but without the substrate, the bilayer graphene). Reorganising the terms, we would have

$$E_{\text{bind}}(\text{I}) = E_{\text{int}}(\text{I}) + E_{\text{elas}}(\text{I})$$

II.II Adhesion

We define the adhesion energy as the loss of energy when the top layer is extracted rigidly from the system:

$$E_{\text{adh}} = -E\left(\text{gr}[\text{I}]_x\right) + E\left(\text{gr}^{\text{T}*}\right) + E\left(\text{gr}^{\text{B}}[\text{I}]_x^*\right)$$

When we add and subtract the same energy terms from this expression, we obtain

$$\begin{aligned}
E_{\text{adh}} &= -E\left(\text{gr}[\text{I}]_x\right) + E\left(\text{gr}^{\text{T}*}\right) + E\left(\text{gr}^{\text{B}}[\text{I}]_x^*\right) + E\left(\text{gr}^*\right) \underline{-E\left(\text{gr}^*\right)} \; \underline{+E(\text{gr})} - E(\text{gr}) \\
&= -E\left(\text{gr}[\text{I}]_x\right) + E\left(\text{gr}^{\text{T}*}\right) + E\left(\text{gr}^{\text{B}}[\text{I}]_x^*\right) + E\left(\text{gr}^*\right) - E_{\text{elas}}(\text{gr}) - E(\text{gr}) \\
&= \underline{-E\left(\text{gr}[\text{I}]_x\right)} + E\left(\text{gr}^{\text{T}*}\right) + E\left(\text{gr}^{\text{B}}[\text{I}]_x^*\right) \; \underline{+E\left(\text{gr}^*\right)} - E_{\text{elas}}(\text{gr}) - E(\text{gr}) \; \underline{+E\left([\text{I}]_x^*\right)} - E\left([\text{I}]_x^*\right) \\
&= -E_{\text{int}} + E\left(\text{gr}^{\text{T}*}\right) + E\left(\text{gr}^{\text{B}}[\text{I}]_x^*\right) - E_{\text{elas}}(\text{gr}) - E(\text{gr}) - E\left([\text{I}]_x^*\right) \\
&= -E_{\text{int}} + E\left(\text{gr}^{\text{T}*}\right) + E\left(\text{gr}^{\text{T}}\right) - E\left(\text{gr}^{\text{T}}\right) + E\left(\text{gr}^{\text{B}}[\text{I}]_x^*\right) - E_{\text{elas}}(\text{gr}) - E(\text{gr}) - E\left([\text{I}]_x^*\right) \; .
\end{aligned}$$

Using the definition $E_{\text{bind}}(\text{gr}) = E(\text{gr}) - E\left(\text{gr}^{\text{T}}\right) - E\left(\text{gr}^{\text{B}}\right), E(\text{gr}) - E\left(\text{gr}^{\text{T}}\right) = E_{\text{bind}}(\text{gr}) + E\left(\text{gr}^{\text{B}}\right)$ and we arrive at

$E_{\text{adh}} = -E_{\text{int}} \underline{+E\left(\text{gr}^{\text{T}*}\right)} \; \underline{-E\left(\text{gr}^{\text{T}}\right)} + E\left(\text{gr}^{\text{B}}[\text{I}]_x^*\right) - E_{\text{elas}}(\text{gr}) - E_{\text{bind}}(\text{gr}) - E\left(\text{gr}^{\text{B}*}\right) - E\left([\text{I}]_x^*\right)$.

Defining the energy differences

$$E_{\text{elas}}\left(\text{gr}^{\text{T}}\right) = -E\left(\text{gr}^{\text{T}}\right) + E\left(\text{gr}^{\text{T}*}\right)$$

and

$$E_{\text{int}}^{\text{B}} = E\left(\text{gr}^{\text{B}}[\text{I}]_x^*\right) - E\left([\text{I}]_x^*\right) - E\left(\text{gr}^{\text{B}*}\right) \; ,$$

which resemble the corresponding energies in the full system, it is easier to work in the relative energies than the absolute ones:

$$\begin{aligned} E_{\mathrm{adh}} &= -E_{\mathrm{int}} + E_{\mathrm{elas}}\left(\mathrm{gr}^{\mathrm{T}}\right) + E_{\mathrm{int}}^{\mathrm{B}} - E_{\mathrm{elas}}(\mathrm{gr}) - E_{\mathrm{bind}}(\mathrm{gr}) \\ &= -\left[E_{\mathrm{int}} + E_{\mathrm{elas}}(\mathrm{gr})\right] + \left[E_{\mathrm{int}}^{\mathrm{B}} + E_{\mathrm{elas}}\left(\mathrm{gr}^{\mathrm{T}}\right)\right] - E_{\mathrm{bind}}(\mathrm{gr}) \end{aligned}$$

Energy components marked blue are negative ("attractive"), the values in red positive ("repulsive"), without the signs included.

Above we defined

$$E_{\mathrm{ic}} = E_{\mathrm{int}} + \left[E_{\mathrm{elas}}(\mathrm{I}) + E_{\mathrm{elas}}(\mathrm{gr})\right],$$

so we have $E_{\mathrm{int}} + E_{\mathrm{elas}}(\mathrm{gr}) = E_{\mathrm{ic}} - E_{\mathrm{elas}}(\mathrm{I})$ and thus we can relate the two energies:

$$E_{\mathrm{adh}} = -E_{\mathrm{ic}} + \left[E_{\mathrm{int}}^{\mathrm{B}} + E_{\mathrm{elas}}\left(\mathrm{gr}^{\mathrm{T}}\right) + E_{\mathrm{elas}}(\mathrm{I})\right] - E_{\mathrm{bind}}(\mathrm{gr}).$$

So we would be left with the two energies, E_{adh} and E_{ic}, with the relation and $E_{\mathrm{bind}}(\mathrm{gr})$, which is the same in all structures (but different in different supercells) and the term in the square brackets.

Further if we take that $E_{\mathrm{elas}}(\mathrm{I})$ is small, as found in practise, we have:

$$E_{\mathrm{adh}} \cong -E_{\mathrm{ic}} + \left[E_{\mathrm{int}}^{\mathrm{B}} + E_{\mathrm{elas}}\left(\mathrm{gr}^{\mathrm{T}}\right)\right] - E_{\mathrm{bind}}(\mathrm{gr}).$$

Another observation of the E_{adh} is that when the top layer is detached from the ions and the bottom layer and is almost flat, $E_{\mathrm{elas}}(\mathrm{gr}) \cong -E_{\mathrm{bind}}(\mathrm{gr})$ and $E_{\mathrm{elas}}\left(\mathrm{gr}^{\mathrm{T}}\right)$ is small, and thus

$$\begin{aligned} E_{\mathrm{adh}} &= -E_{\mathrm{int}} + E_{\mathrm{elas}}\left(\mathrm{gr}^{\mathrm{T}}\right) + E_{\mathrm{int}}^{\mathrm{B}} - E_{\mathrm{elas}}(\mathrm{gr}) - E_{\mathrm{bind}}(\mathrm{gr}) \\ &\cong -E_{\mathrm{int}} + E_{\mathrm{int}}^{\mathrm{B}}. \end{aligned}$$

Indeed we find that the sum of the latter two terms approaches the value of the E_{adh}, in particular in the system 3-ClO_4^--L, where the assumptions are nearly fulfilled:

$$E_{\mathrm{adh}} = 2.67\ \mathrm{eV}, -E_{\mathrm{int}} + E_{\mathrm{int}}^{\mathrm{B}} = 2.18\ \mathrm{eV}$$

III Supplementary Note 2: Effect of the Surface Area

Note: In the structures presented below, we have inserted anions into two additional different supercells in the same manner as in the 12×12 supercells. We have added a number before each structure to distinguish between them. This number corresponds to the size of the supercell used. For example, if a single anion is inserted into a 10×10 supercell, the structure will be named 10-1-ClO_4^- to indicate the specific structure being referred to.

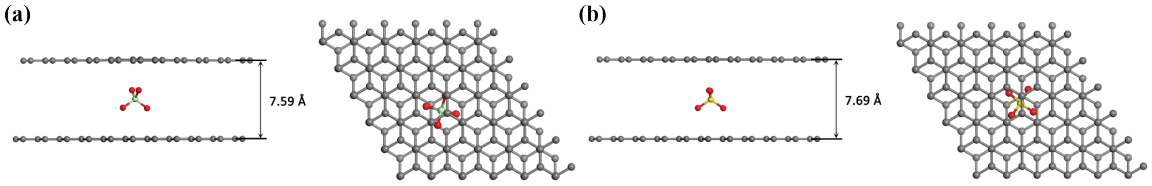

Figure S8: Anions intercalated between 6×6 bilayer graphene. Side and top view of (a) 6-1-ClO_4^- and (b) 6-1-SO_4^{2-}.

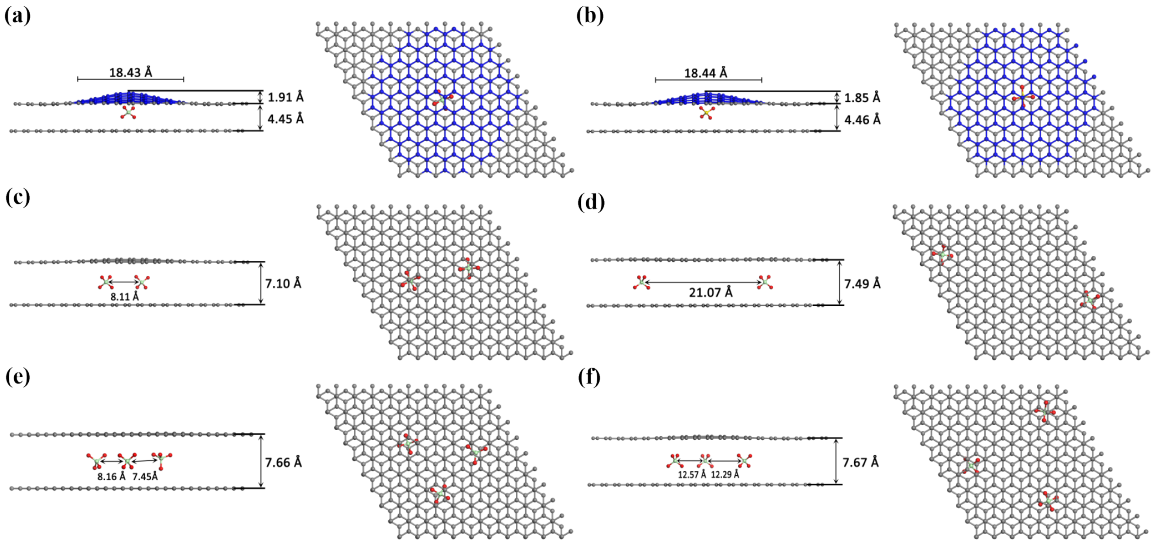

Figure S9: Anions intercalated between 10×10 bilayer graphene. Side and top view of (a) 10-1-ClO_4^-, (b) 10-1-SO_4^{2-}, (c) 10-2-ClO_4^--S, (d) 10-2-ClO_4^--L, (e) 10-3-ClO_4^--S, and (f) 10-3-ClO_4^--L.

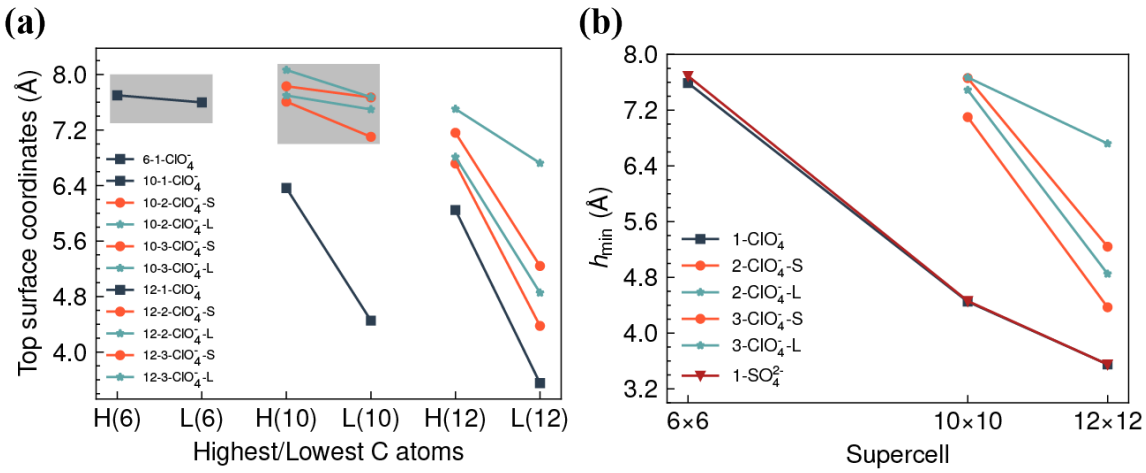

Figure S10: (a) Vertical coordinates of the highest and lowest C atoms of the upper layer of all structures. The gray shades indicates that the difference between the highest and lowest carbon atoms is less than 0.49 Å. (b) The variation in $h_{\min}$ against different supercells: 6×6, 10×10, and 12×12.

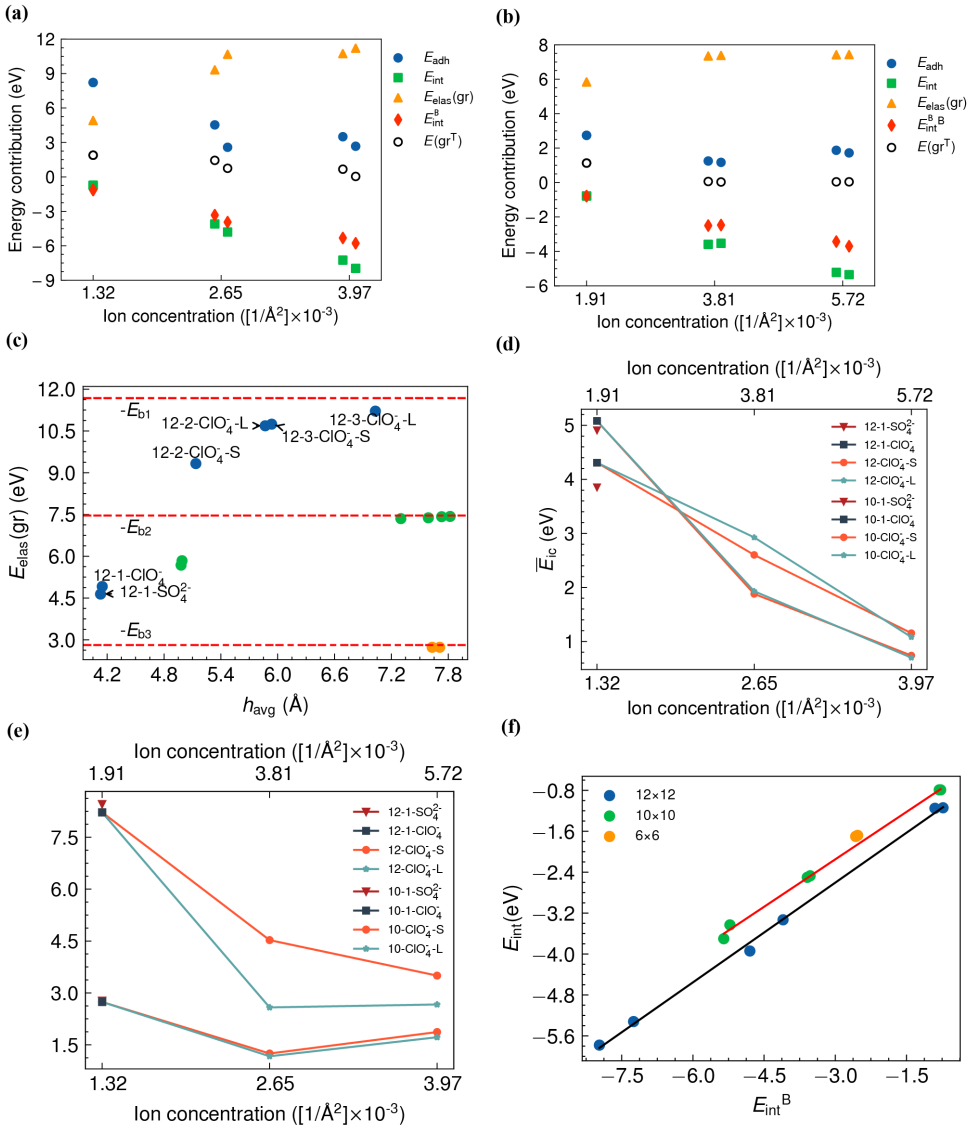

Figure S11: Adhesion energy (E_{adh}) and its contributions as a function of the ion concentration in (a) 12×12 and (b) 10×10. (c) Elastic energy (E_{elas}(gr)) as a function of the average height (h_{avg}) in 12×12, 10×10, and 6×6. The E_{b1}, E_{b2} and E_{b3} are the binding energies of the 12×12, 10×10, and 6×6 pristine bilayer graphene, respectively. (d) The intercalation energy per anion, and (e) the adhesion energy in 12×12 and 10×10, and (f) the relationship between the intercalation energy (E_{int}) and the interaction between the ions and the bottom layer ($E^{\mathrm{B}}_{\mathrm{int}}$) in 12×12, 10×10, and 6×6. As mentioned in the main text, the ion concentration C is given by $C = \frac{n}{A}$, where C represents the ion concentration, n denotes the number of ions, and A represents the area in angstroms. In Figures (d) and (e), the ion concentrations for the 12×12 and 10×10 cells are represented on the lower and top x-axes, respectively.

Table S3: Energetic and Structural Characteristics of Intercalated Systems: 6×6, 10×10, and 12×12. Adhesion Energy (E_{adh}), Intercalation Energy per Anion $\left(\bar{E}_{\mathrm{ic}}\right)$, Total Intercalation Energy (E_{ic}), Elastic Energy of the Bilayer Graphene (E_{elas} (gr)), Interaction Energy (E_{int} (gr[I]$_{\mathrm{x}}$)), The Energy Cost to Create the Nanoprotrusion $\left(E_{\mathrm{elas}}\left(\mathrm{gr}^{\mathrm{T}}\right)\right)$, The Interaction Between the Ions and the Bottom Layer $\left(E_{\mathrm{int}}^{\mathrm{B}}\right)$, Minimum Interlayer Distance (h_{min}), Average Height of the Top Layer (h_{avg}), and Nano-protrusion Height (h_{nano}). All Energies are Expressed in eV and heights in Å.

Structures	E_{adh}	$\bar{E}_{\mathrm{ic}}$	E_{ic}	E_{elas}(gr)	E_{int} (gr[I]$_x$)	$E_{\mathrm{elas}}\left(\mathrm{gr}^{\mathrm{T}}\right)$	$E_{\mathrm{int}}^{\mathrm{B}}$	h_{min}	h_{avg}	h_{nano}
6-1-SO_4^{2-}	0.92	0.19	0.19	2.73	-2.53	0	-1.68	7.69	7.71	0
6-1-ClO_4^-	0.94	0.18	0.18	2.73	-2.57	0	-1.70	7.59	7.63	0
10-1-SO_4^{2-}	2.78	4.91	4.91	5.68	-0.81	0.98	-0.79	4.46	4.98	1.85
10-1-ClO_4^-	2.74	5.08	5.08	5.84	-0.78	1.13	-0.79	4.45	4.99	1.91
10-2-ClO_4^--S	1.25	1.88	3.77	7.35	-3.59	0.06	-2.50	7.10	7.30	0
10-2-ClO_4^--L	1.17	1.93	3.86	7.38	-3.53	0.03	-2.47	7.49	7.59	0
10-3-ClO_4^--S	1.87	0.74	2.21	7.42	-5.22	0.04	-3.43	7.66	7.73	0
10-3-ClO_4^--L	1.72	0.70	2.10	7.43	-5.35	0.04	-3.70	7.77	7.82	0
12-1-SO_4^{2-}	8.46	3.85	3.85	4.64	-0.90	1.70	-1.15	3.55	4.13	2.43
12-1-ClO_4^-	8.22	4.31	4.31	4.91	-0.73	1.89	-1.14	3.55	4.15	2.49
12-2-ClO_4^--S	4.53	2.60	5.20	9.33	-4.10	1.44	-3.33	4.37	5.14	2.34
12-2-ClO_4^--L	2.58	2.93	5.85	10.68	-4.80	0.75	-3.94	4.88	5.87	0.90,0.90
12-3-ClO_4^--S	3.50	1.15	3.46	10.74	-7.25	0.67	-5.32	5.24	5.94	1.92
12-3-ClO_4^--L	2.67	1.08	3.24	11.21	-7.97	0.04	-5.78	6.72	7.03	0.78

Intuitively, one might expect that changing the coverage area of the structures could affect the interaction of anions with graphene layers. To explore this idea, we conducted a series of additional DFT calculations. These were designed to determine how the interaction of confined anions with bilayer graphene is influenced by manipulating both the ion concentration and distance between inserted anions, as well as the area of the graphene surface. The aim is to understand how these factors influence the properties of the systems. Figures S8 and S9 show two distinct graphene supercells, the 6×6 and 10×10 structures. These are set in comparison with the 12×12 structure, which has been examined in the main text. Upon the intercalation of single ClO_4^- and SO_4^{2-} ions into the 6×6 cell, the upper surface was shifts in the z-direction, thereby increasing the spacing between graphene layers without inducing any surface deformation (nano-protrusion), as depicted in Figure S8. After relaxation, the anions maintained their bond lengths between atoms, comparable to those in the gas phase. The h_{min} were measured to be 7.59 and 7.69 Å for ClO_4^- and SO_4^{2-} respectively. This expansion is anticipated given the small surface area of the graphene and the large volume of the inserted anions, which apply a uniform stress across the entire top layer. This consequently reduces the van der Waals forces between graphene layers, facilitating ion intercalation. The h_{min} values obtained herein for ClO_4^- and SO_4^{2-} closely aligned with previous findings [1, 2]. The slight discrepancy between our results and those reported can be attributed to the different functionals and approaches employed in our study. The variation in h_{min} induced by SO_4^{2-} intercalation is due to its slightly larger volume compared to ClO_4^-. Indeed, several studies have reported that the graphite interlayer expands as the molecular volume or ionic radius of the intercalate increases [1, 3, 4]. This is only the case when the lateral size of the supercells is small, as noted in the main text for the 12×12 system, where the variation in the molecular volume exerted a negligible effect. As illustrated in Figure S9, the intercalation behavior of single ClO_4^- and SO_4^{2-} ions in the 10×10 structure was analogous to that of the single anion in the 12×12 structure. The top layer exhibited slight bending at the edges, leading to interaction between the graphene layers. Consequently, the top sheet moved closer to the bottom, forming a nano-protrusion. The values for 10-1-ClO_4^- were lower by 0.58 Å for h_{nano} and 0.9 Å for h_{min} compared to 12-1-ClO_4^-. Similar values were observed for SO_4^{2-} when compared with 12-1-SO_4^{2-}. When a single anion was inserted into the 12×12 structure, the spacing between

the layers was less than 4 Å, suggesting that a limited ion concentration were insufficient to induce substantial intercalation. In contrast, a larger spacing was obtained for 1-6-ClO_4^-. As the supercell size of the bilayer graphene was reduced, the layers are able to separate further apart, resulting in an increase in $h_{\min}$, as shown in Figure S10(b). We increased the ion concentration in the 10×10 structure following the same methodology as that discussed for the 12×12 structure. Intriguingly, upon intercalation of additional anions, as depicted in Figures S9(c) and (d), the two anions, irrespective of their distances, readily overcame the weakly bonded bilayer graphene. This resulted in a high $h_{\min}$ exceeding 7 Å, with no nano-protrusion on the surface. Only minor warping is observed, as illustrated in Figure S10(a). Ref. [5] also reported the separation of interaction between stacked graphene layers due to intercalation. According to their calculations, the intercalation of a large number of SO_4^{2-} ions, forming a monolayer, separated the graphene layers by 7.6 Å and decoupled the electronic interaction between them. The minimal distortion of the bilayer graphene basal planes and the large inter-atomic distances between the O and C atoms suggest the absence of strong covalent interaction between the oxygen electrons and the π electrons of the graphene layers. The $h_{\min}$ slightly increases to a value of 7.66 Å when three closely packed anions are intercalated (Figure S9e). However, beyond this point, despite the large distance between the anions, the $h_{\min}$ remains relatively constant (Figure S9f). This suggests that further increasing the ion concentration fails to increase the graphene spacing. In our previous study [6] and in Ref. [7], it was found that the number of hydroxide ions decreases as the SO_4^{2-} concentration rises, leading to low water content. Consequently, the graphite expansion and anion intercalation processes are expected to proceed slowly. Nevertheless, our theoretical results revealed that the distance between the graphene layers reached a maximum, even with a relatively large ion concentration.

In terms of energetics, the $\bar{E}_{\text{ic}}$ of the structures decreases as the ion concentration increases, similar to the trend observed in the 12×12 structure, where the initial intercalation requires more energy than subsequent intercalations, as depicted in Figure S11 (d). Conversely, the E_{adh} exhibits relatively minor changes with an increasing ion concentration, as shown in Figure S11 (e). To gain a deeper understanding of these trends, we will discuss the decomposition of energies for both quantities, while concurrently drawing parallels with the 12×12 structures.

All systems exhibit a negligible $E_{\text{elas}}(\text{I})$. As a result, the intercalation energy is governed by the competition between the elastic ($E_{\text{elas}}(\text{gr})$) and ($E_{\text{int}}\,(\text{gr}[\text{I}]_x)$) interaction energies. In terms of $E_{\text{elas}}(\text{gr})$, when multiple anions are inserted, the distance between the ions becomes less relevant in smaller cells. The resulting values are essentially identical and closely align with the limiting value of the binding energy of pristine 10×10 bilayer graphene. In this state, the upper layer detaches, eliminating interaction between the layers, as depicted in Figure S11 (c) and Table S3. However, when comparing the 10×10 to the 12×12 structure with a single anion, the $E_{\text{elas}}(\text{gr})$ for the 10-1-ClO4$^-$ structure is larger due to the greater h_{min}, which results in the layer being elevated uniformly, which costs more $E_{\text{elas}}(\text{gr})$. This occurs regardless of the size of the nano-protrusion, as the systems lose more of the interaction energy between the graphene layers in the 10-1-ClO_4^- structure. This is evident in Table S3 when comparing 12-2-ClO_4^--L and 12-3-ClO_4^--S, where the latter has a larger h_{nano} and h_{min}, and nearly identical h_{avg}, yet they possess the same $E_{\text{elas}}(\text{gr})$. However, when comparing 10-1-ClO_4^- with 12-2-ClO_4^--S, the h_{avg} is nearly the same, but the $E_{\text{elas}}(\text{gr})$ is significantly higher by about 3 eV. This might be attributed to the fact that the 12×12 cell has a 44% larger area than the 10×10 cell. From these results, we can conclude that the elastic energy is an extensive quantity and depends on three factors: the h_{min}, the h_{nano}, and the surface area of the systems (Figure S11 (c) and Table S3).

The values of $E_{\text{int}}\,(\text{gr}[\text{I}]_x)$ demonstrate that the anions have a significant attractive interaction with the graphene layers, as shown in Table S3. This aligns with the behavior of the charge transfer between anions and the graphene layers, which is similar in both 10×10 and 12×12 structures. Therefore, as the ion concentration increases, the electron transfer between the anions and bilayer graphene is expected to increase. This results in a higher energetic cost and overall energy, which explains the greater challenge for a single anion to intercalate, while it is easier for multiple anions. Thus, the ease of anion intercalation into bilayer graphene appears to be influenced by the extent of electron transfer.

Regarding $E_{\text{elas}}\left(\text{gr}^{\text{T}}\right)$, the energy cost to create a nano-protrusion is approximately 1 eV for a single anion when intercalated in the 10×10 cell. This cost becomes negligible for other cases involving 2 or 3 anions (cases S or L), as no nano-protrusion is generated on the surface. For instance, when these structures are compared to the 12-3-ClO_4^--L system, similar values are observed, despite the $h_{nano} = 0.78$ Å (Table S3). Such similarity

arises because the elevation is distributed over a large area, and the small local curvature does not incur significant energy cost. In Figure S11 (f), the $E_{\text{int}}^{\text{B}}$ is plotted against the total interaction, revealing a strong correlation. The energy $E_{\text{int}}^{\text{B}}$ represents the interaction between the ions and the bottom layer. One might expect that the $E_{\text{int}}^{\text{B}}$ would be half of the total interaction, given that only the two oxygens facing the bottom layer interact with it. Yet, this is not the case. The discrepancy could be attributed to the fact that the bottom layer is fixed, causing the entire electron structure to adjust accordingly. This might explain why the slope in the figure is not equal to one.

The E_{adh} trend across all structures, both 12×12 and 10×10, is primarily influenced by the elastic energy. It becomes saturated immediately following the incorporation of multiple anions into the 10×10 structures, in comparison with the 12×12 structures, as depicted in Figures S10 (a) and (b). The E_{elas}(gr) values, hover around 7.40 eV when either 2 or 3 anions are intercalated (cases S or L). Interestingly, these values are close in magnitude to the binding energy of the pristine 10×10 bilayer graphene, which is -7.46 eV (Table S3). This is due to the high separation induced between graphene layers during intercalation. The presence of multiple anions causes the upper layer to become flat, resulting in the loss of attractive interactions between the layers.

IV Supplementary Note 3: Effect of Microsolvation

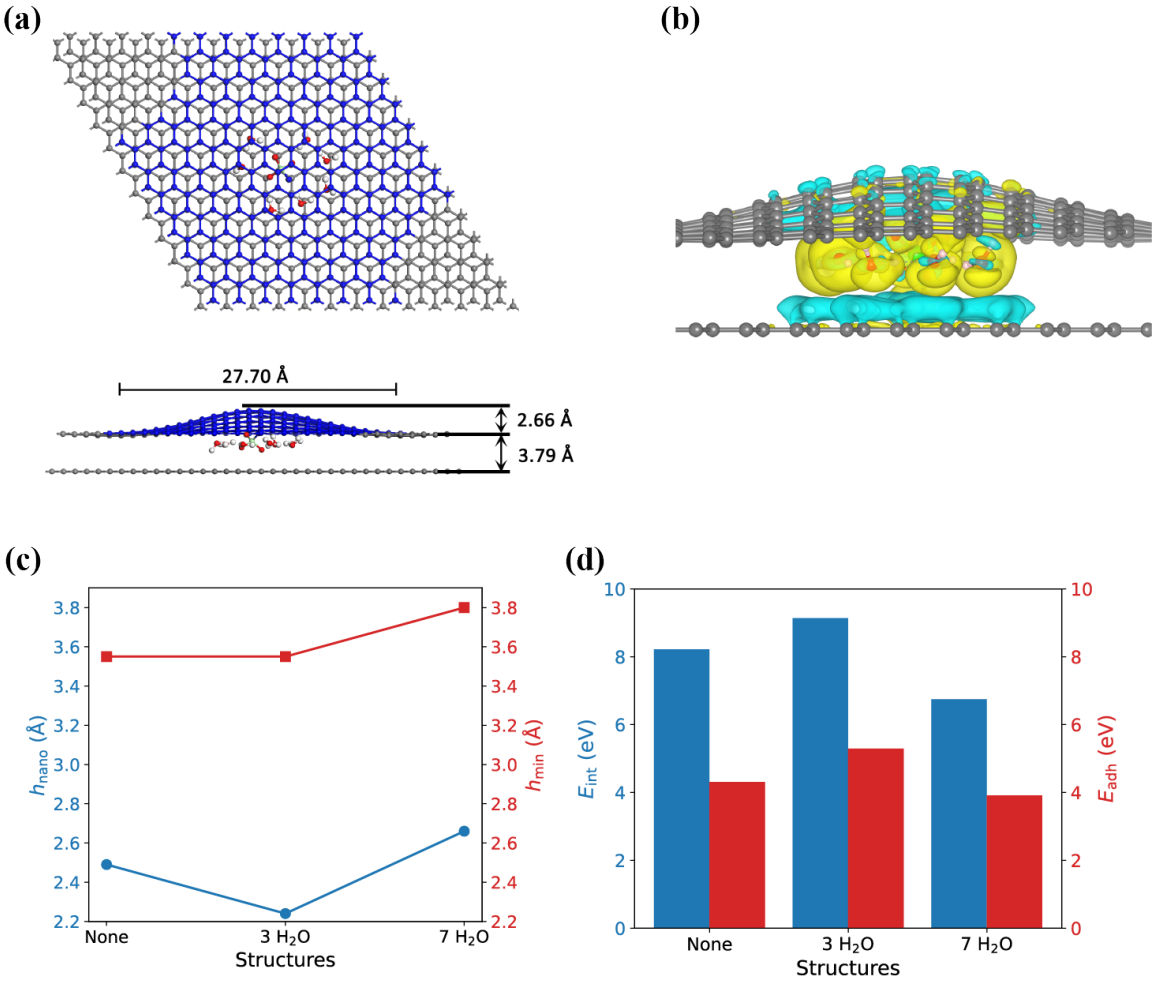

Figure S12: (a) DFT model of single ClO_4^- anion surrounded by seven water molecules intercalated between two graphene layers; top and side view with the blue atoms indicating the deformed graphene region and (b) the charge density difference. (c) The h_{min} and the h_{nano} for three different structures: None represents the 1-ClO_4^- structure without solvation shell, 3-H_2O represents 1-ClO_4^--3-H_2O, and 7-H_2O represents 1-ClO_4^--7-H_2O. (d) The E_{ic} and E_{adh} for the three structures.

Table S4: Bader Charges for the Intercalated Bilayer Graphene Solvated Anion Systems

Structures	Sum over C atoms	Top layer	Bottom layer	Sum over ClO_4^-	Avg. over O atoms	Cl atoms
Pristine bilayer	-0.003	-0.002	-0.001	-	-	-
ClO_4 neutral	-	-	-	0	-0.602	2.410
1-ClO_4^-	0.864	0.370	0.494	-0.867	-0.842	2.502
1-ClO_4^--3-H_2O	1.423	0.736	0.686	-1.387	-0.691	1.377
1-ClO_4^--7-H_2O	0.972	0.302	0.670	-0.873	-0.842	2.497

Under practical experimental conditions, water molecules may co-intercalate with the anions during the intercalation mechanism within the graphitic layers. In fact, the possibility of ion-solvent intercalation has been reported from previous experiments [2, 7, 8]. These studies demonstrated that as graphite layers undergo oxidation, they depolarize and expand, thereby facilitating the intercalation of anionic species and potential co-intercalation of water molecules. To this end, we made an initial attempt to quantitatively verify the effect of incorporating water molecules as microsolvation of ClO_4^- on the graphene surface. We constructed a model where several H_2O molecules surrounded the ClO_4^- anions in between the bilayer graphene. An explicit solvent model was used, and the number of water molecules was determined based on earlier studies [9, 10, 11]. These studies had determined that tetrahedral anions, such as SO_4^{2-}, exhibit stability when coordinated with a minimum of three water molecules depending on the concentration. In the models herein, we have used the minimum of three and a maximum of seven water molecules to construct a two-dimensional hydrated cluster surrounding the ClO_4^-. This approach offers an appropriate model to elucidate the molecular interaction between the ion-solvent and graphene surfaces. In Figure S12a, we illustrate a model of the 1-ClO_4^--7-H_2O system, where the ClO_4^- anion is surrounded by seven water molecules as example. The introduction of H_2O leads to substantial changes in various properties. For example, as depicted in Figures S12c, the h_{nano} decreases with the presence of three water molecules but increases when seven are present. This can be attributed to the reduced interaction between the top layer and the anion and the enhanced interaction between the anion and water molecules when fewer H_2O molecules are present, resulting in a lower protrusion. In contrast, when the number of water molecules is larger, they predominantly interact with each other rather than the anion. This phenomenon is evident in the charge distribution, as the charges for the Cl and O atoms differ markedly from the cases without solvation or with seven water molecules. In the absence of solvent, the E_{ic} was determined to be 4.31 eV. However, with the inclusion of H_2O molecules, E_{ic} initially rises to 5.30 eV before decreasing to 3.91 eV. This trend suggests that a larger number of water molecules could be advantageous for the intercalation process, potentially due to an increase in charge transfer between the host material and intercalants. Concurrently, the E_{adh} increases from 8.21 to 9.14 eV and subsequently drops to 6.75 eV. The adhesion of the top graphene layer is significantly influenced

by H_2O and could facilitate local exfoliation of the graphene surface. The maximum charge transfer from graphene to the solvated anion is greater in the 1-ClO_4^--7-H_2O system, but the amount of charge acquired by ClO_4^- is nearly identical to that in the unsolvated case Table S3. The remaining charges are lost from the graphene π-system and gained by the water molecules. This observation implies that charge transfer from graphene layers to anions plays a crucial role and suggests that the intercalation process relies on charge transfer between intercalants and graphene layers as shown also in the main text. Based on our calculations and comparisons with structural parameters obtained from STM, we propose that, during the early stages of the intercalation mechanism, only the anion, without the solvation shell, occupies the interlayer space, inducing surface deformation and expanding the spacing, which may subsequently be followed by solvent molecules.

References

[1] Ken Tasaki. Density functional theory study on structural and energetic characteristics of graphite intercalation compounds. *The Journal of Physical Chemistry C*, 118(3): 1443–1450, 2014.

[2] Hoyoung Lee, Ji Il Choi, Jinho Park, Seung Soon Jang, and Seung Woo Lee. Role of anions on electrochemical exfoliation of graphite into graphene in aqueous acids. *Carbon*, 167:816–825, 2020.

[3] Kolja Beltrop, Paul Meister, Sven Klein, Andreas Heckmann, Mariano Grünebaum, Hans-Dieter Wiemhöfer, Martin Winter, and Tobias Placke. Does size really matter? new insights into the intercalation behavior of anions into a graphite-based positive electrode for dual-ion batteries. *Electrochimica acta*, 209:44–55, 2016.

[4] Olena Lenchuk, Philipp Adelhelm, and Doreen Mollenhauer. New insights into the origin of unstable sodium graphite intercalation compounds. *Physical Chemistry Chemical Physics*, 21(35):19378–19390, 2019.

[5] Isabe G Ayala, Nicolas A Cordero, and Julio A Alonso. Surfactant effect of sulfuric acid on the exfoliation of bilayer graphene. *Physical Review B*, 84(16):165424, 2011.

[6] Stefania De Rosa, Paolo Branchini, Rossella Yivlialin, Lamberto Duo, Gianlorenzo Bussetti, and Luca Tortora. Disclosing the graphite surface chemistry in acid solutions for anion intercalation. *ACS Applied Nano Materials*, 3(1):691–698, 2019.

[7] Khaled Parvez, Zhong-Shuai Wu, Rongjin Li, Xianjie Liu, Robert Graf, Xinliang Feng, and Klaus Mullen. Exfoliation of graphite into graphene in aqueous solutions of inorganic salts. *Journal of the American Chemical Society*, 136(16):6083–6091, 2014.

[8] Zhaodong Huang, Yue Hou, Tairan Wang, Yuwei Zhao, Guojin Liang, Xinliang Li, Ying Guo, Qi Yang, Ze Chen, Qing Li, et al. Manipulating anion intercalation enables a high-voltage aqueous dual ion battery. *Nature Communications*, 12(1):3106, 2021.

[9] Xue-Bin Wang, John B Nicholas, and Lai-Sheng Wang. Electronic instability of isolated so 4 2- and its solvation stabilization. *The Journal of Chemical Physics*, 113(24):10837–10840, 2000.

[10] Manel Canales and Elvira Guardia. Water-water and ion-water hydrogen bonding in sulfuric acid solutions. *Journal of Molecular Liquids*, 293:111463, 2019.

[11] Quan Wan, Leonardo Spanu, Francois Gygi, and Giulia Galli. Electronic structure of aqueous sulfuric acid from first-principles simulations with hybrid functionals. *The Journal of Physical Chemistry Letters*, 5(15):2562–2567, 2014.